

# **Electrochemical Properties of Diamond Electrode Materials**

Christopher J Harris  
Department of Chemistry  
University of Maine

---

## ***Abstract***

The first part of this paper examines the historical evolution of diamond film growth through the eyes of a material scientist. The selective etching behavior of atomic hydrogen gives rise to metastable diamond films. The second portion explores why diamond electrodes hold so much promise on the electrochemical front. Hardness, chemical inertness, and optical transparency give it superior properties no other material can match.

---

## ***Introduction***

Figure 1 depicts the origins and potential rewards of diamond research in the form of a "diamond technology tree". Such rewards include: hardness coatings, biocompatible materials, heat sinks, chemical resistance, optical applications, acoustic properties, and semiconductor devices. For comparison purposes, a diamond computer could operate about ten times faster than an equivalent silicon computer. More specifically, figure 2 shows how diamond electronic properties measure up to silicon and beta-silicon carbide. Diamond possesses superior carrier mobility, thermal conductivity, and hardness characteristics over silicon or beta-silicon carbide.

As a general rule, high pressure/high temperature man-made diamonds have more impurities and defects than natural diamonds. Within the natural diamond spectrum, less than 10 % qualify for semiconductor standards based on impurities and defects. With a low pressure environment, vapor processes take place, rather than direct solid/ solid

phase transitions, controlling the growth process in such a way that impurities and defects can be minimized, in a metastable growth regime.

At this point, it's instructive to see how other people have attempted vapor deposition diamond. A comprehensive review and comparison of vapor methods with their associated diamond film properties are given by Deshpandey and Bunshah[1]. Basically there are three general categories: 1) thermal chemical vapor deposition(CVD), 2) plasma assisted CVD, and 3) ion assisted physical vapor deposition(PVD). Most techniques involve supersaturation of atomic hydrogen, particularly the first two chemical processes. Now each of these categories will be considered individually.

Thermal CVD contains three subdivisions: i) chemical vapor transport, ii) hot filament CVD, and iii) electron assisted CVD. Schematics illustrating these methods appear in figure 3. Historically, chemical vapor transport was the first continuous vapor technique ever tried. Gas sources were typically methane and molecular hydrogen. From these preliminary experiments, it became clear that a supersaturation of atomic hydrogen was necessary to "catalyze" the growth process. Subsequently, hot filament CVD offered a more convenient way to achieve diamond growth. The filament served to crack the methane and molecular hydrogen into carbon precursors and atomic hydrogen. Electron assisted CVD has essentially the same set-up as hot filament CVD, but the substrate is biased positive to provide enhanced electron bombardment on the film surface.

An alternative approach for obtaining carbon precursors and atomic hydrogen involves a plasma source instead of a filament. Again, methane and molecular hydrogen provide the essential ingredients to achieve diamond; however, the gas sources in plasmas are quite a bit more flexible than thermal CVD approaches. Because plasma assisted CVD is by far the most popular method in growing diamond, figure 4 only scratches the surface of possible deposition configurations. Plasma excitation sources include: hollow cathode, direct current(DC), radio frequency(RF), microwave, and magneto assisted microwave.

Physical vaporization of graphite while bombarding the substrate with ions has shown very little hope for diamond deposition, despite its success in obtaining other metastable films. As an example, ion bombardment has stabilized the metastable growth of cubic-BN from a BN target[2]. Evaporant or sputter sources range from: lasers, ion beams, pulse discharge rail guns, or plasmas. Ion bombardment of the substrate can originate from the primary sputter source or independently provided through secondary plasmas or ion beams. A number of variations appear in figure 5.

Lately, a few new techniques have emerged, such as thermal plasma assisted CVD, UV enhanced CVD, and acetylene torch pyrolysis; however, these approaches have only improved growth rates while sacrificing film quality. By far the cheapest method, the acetylene torch apparatus cost less than \$100 to construct! More importantly, these alternative methods offer insight into the diverse nature of diamond growth. Currently, no techniques yield heteroepitaxy, although many approaches achieve epitaxy on diamond or polycrystalline films on foreign substrates.

### ***Metastability***

A common phase diagram for carbon is depicted in figure 6. At a typical substrate temperature of 1000 C, a pressure of 40,000 atm would be required to grow thermodynamically stable diamond. Finding chemical precursors and technology to build such a system in this thermodynamic regime pose major obstacles. Instead, most people have chosen to grow in the metastable regime at subatmospheric pressures where gaseous reactants can be utilized. Ultra high vacuum systems minimize the level of contaminants present and surface chemical reactions control the growthrate. These measures are intended to minimize the defects present in the final product.

Although diamond is thermodynamically unstable compared to graphite, the free energy difference is only .03 eV/atom (approximately kT) at room temperature and pressure. Since diamond and graphite exist in deep potential wells, the activation energy between them appears to be high. Also, the energy spread between solid carbon and free

atoms in the gas phase is 7 eV/atom, a substantial difference. Hence, once the metastable diamond is formed, transformation to graphite or gas phase is negligible unless subjected to high temperatures[3].

Surface phenomenon may influence diamond versus graphite formation. Metastable allotropes of other materials have been stabilized on substrates of same or different bonding type. Figure 7 lists some favorable examples found in the literature. The key factor involves interfacial energies for both substrate-film systems. It is conceivable that the interfacial energy is less for the metastable phase despite its larger bulk free energy. For instance, lattice match between the substrate and film could push the overall free energy in favor of the metastable phase for thin films[4]. This thermodynamic rationale may offer insight into the presence or absence of buffer layers as different substrate conditions prevail.

### ***Structure***

Carbon has such unique characteristics that the whole field of organic chemistry evolved to explain its nature. Its compact radius and tetravalent electron shell allow bonding angles and packing densities unparalleled by any other element in the periodic table. In light of this, it's not surprising that carbon alone can exist in a variety of allotropes such as: amorphous carbon, glassy carbon, microcrystalline carbon, graphitic carbon, diamond-like carbon, and diamond. Although the differences appear to be a matter of definition, the variations stem from the relative populations of  $sp^3$ ,  $sp^2$ ,  $sp^1$  hybridized orbital states and impurity levels[3,5]. Since diamond and graphite represent the purest forms of  $sp^3$  and  $sp^2$  hybridization, respectively, let's consider their structure in more detail.

Most semiconductor people like to visualize diamond in terms of two face centered cubic lattices displaced by one quarter of the cube diagonal. Unfortunately, this description gives very little perspective about the surface structure which is important when considering reaction mechanisms. Alternatively, one could view diamond as

stacked layers of cyclohexane-type rings, each in the "chair" conformation. If the chair layers are joined by staggered carbon-carbon bonds, the six-membered rings between layers become chairs as in figure 8. This staggered configuration results in an ABC/ABC/... stacking sequence in the <111> direction. On the other hand, if chair layers are joined by eclipsed carbon-carbon bonds, "boat" type rings interconnect layers and an AB/AB/AB... stacking sequence results. Figure 9 depicts the eclipsed version, properly known as lonsdaleite. The eclipsed bonds enhance next-nearest neighbor repulsive forces which make it less energetically favorable relative to diamond[3].

Graphite, figure 10, possesses layers of benzene-style rings on the horizontal plane and a loosely bound pi network between planes. Surprisingly, no one can fully explain the nature of this pi network. Some people have compared it to van der Waals attraction or weak end-to-end overlap of p<sub>z</sub> orbitals; however, no description seems to fit. The pi network arises from the extra valence electron associated with each carbon atom which contribute to a delocalized orbital. These delocalized orbitals between the planes are responsible for graphite's characteristic electrical conductivity and dark color[3].

No structure section would be complete without mention of a "working definition" for characterizing diamond films. Badzian feels genuine diamond films should have:

- "(i) a crystalline morphology discernible by electron microscopy(SEM/TEM);*
- (ii) a single phase crystalline structure identified by x-ray and/or electron diffraction;*
- (iii) a Raman spectrum typical for diamond, i.e. a single narrow line at 1332 cm<sup>-1</sup> [6]."*

Since any further discussion of characterization would dilute the focus of this paper, the reader should appeal to references [6] and [7] for more details.

### ***Nucleation and growth***

As the introduction previewed, a wide spectrum of techniques are presently

available for the vapor deposition of diamond, including: hot filament[7], microwave plasma[7], DC plasma[8], laser-induced[9], magneto-microwave plasma[10], and RF induction thermal plasma[11]. The questions raised about diamond have shifted from which method will work to what chemical environment provides the most favorable growth conditions. Factors that dramatically influence the chemical environment, involve: gaseous intermediates, energy profile, substrate material, surface cleanliness, and substrate topography. Although research has progressed on these issues, the results are still quite sketchy. The upcoming text will offer current perspectives.

The Russians did some preliminary thermodynamic analysis of diamond comparing chemical crystallization (CVD) to physical crystallization (PVD). Although it would be futile to repeat the derivation here; supersaturation coefficients, latent heats of evaporation, and chemical equilibrium constants reveal that supersaturation levels in CVD can be substantially lower than PVD, assuming comparable growthrates. If defect density can be attributed to supersaturation levels, then CVD should yield purer crystals than PVD. As an example, the Russians drew from tungsten literature. Apparently, hydrogen reduction of tungsten fluoride produced single crystalline tungsten layers at 850 C; whereas, physical vaporization did not lead to similar results[12]. Subsequently, experiments have shown with the case of diamond, CVD produces superior films to physical vaporization of graphite.

On the experimental front, the Russians developed the first continuous vapor process using chemical vapor transport. The apparatus was a closed system containing graphite, a substrate, and hydrogen gas. They applied heat to the system either thermally or via electrical discharge. Under heated conditions, the hydrogen reacted with the graphite to form hydrocarbons which diffused over to the substrate[12]. During this early work, the Russians noted that diamond could be selectively grown on the substrate by increasing the concentration of atomic hydrogen. Whether the superequilibrium amounts of atomic hydrogen came from thermal sources or electric discharge, it preferentially etched away graphite more effectively than diamond as the film grew on the substrate. In addition, the

Russians found that atomic hydrogen interacted with hydrocarbons adsorbed on the substrate and in the gas phase. Therefore, atomic hydrogen played an active role as an etchant and a catalyst in the growth process[12].

As a first pass, the Russians tried to grow diamond on diamond crystals. At a substrate temperature of 600 C, polycrystalline layers with grain sizes in the range of 20 angstroms were obtained. After further research, they found a threshold at 750 C where "high-perfection single-crystalline layers" could be deposited on the {110} face of natural diamond. Above 750 C, growthrate increased until it saturated out at about 1000 C. Going beyond 1000 C, the researchers learned that the growthrate deteriorated and electron diffraction revealed graphite inclusions[12].

Surprisingly, stress increased by a factor of three as the growth temperature was lowered from 1100 to 800 C. With the scrutiny of an electron microscope, stresses in homoepitaxial films appear to be linked with void-type defects incorporated during growth. If the stress between the substrate and the film exceed a certain limit, voids and microtwins develop throughout growth. Under high stress conditions, electron spin resonance measurements show broken C-C bonds within the film. Although the origins of stress remain unclear, the Russians conclude that during high crystallization rates, diamond morphology shifts from single-crystalline to polycrystalline as stress increases [12].

Time passed and the Russians ventured into the realm of foreign substrates. Despite concerted efforts to achieve heteroepitaxy, the research team could only attain polycrystalline films. Nucleation rates, which were determined by counting crystals, varied from  $10^3$  to  $10^8$  per  $\text{cm}^2 \cdot \text{h}$ , depending on growth conditions, substrate material, and substrate preparation. Spontaneous nucleation of diamond crystals was principally observed on defects like scratches, grain boundaries, and dislocation steps. Therefore, polishing the substrate prior to growth tended to enhance nucleation; whereas, annealing tended to suppress nucleation. For carbide forming surfaces, such as Si, Mo, and W, nucleation increased by one to two orders of magnitude, relative to non-carbide forming

surfaces, such as Cu and Au. The presence of grain boundaries on polycrystalline substrates favored nucleation in comparison to single-crystalline surfaces of the same material[12]. Here, the trends conform to the laws of thermodynamics if you take into account the surface free energy.

Diamond crystals grown on non-carbide forming substrates exhibited shapes resembling half-polyhedra pictorially shown in figure 11. Under an optical microscope, crystal habit could be identified and linear measurements in the  $<100>$  and  $<111>$  directions gave rise to growth ratio,  $v_{100}/v_{111}$ . Low supersaturation levels yield cubic shape ( $v_{100}/v_{111} < .6$ ), intermediate supersaturation levels produce cubo-octahedral forms, and high supersaturation levels favor octahedral habit ( $v_{100}/v_{111} > 3$ ). Figure 12 illustrates crystal habit as a function of supersaturation by plotting growth ratio versus substrate temperature[12].

In polycrystalline films, twins have been observed to propagate as early as the nucleation stage right through later stages of growth. Twinning probability, as high as 50 % of crystals nucleated, has been shown to increase with supersaturation, consistent with the preliminary thermodynamic analysis. Consequently, twinning constrains polycrystalline grain size to less than 100 micrometers if realistic growthrates of 1 micrometer/hour are desired[12].

The next meaningful development came out of Stanford, where natural diamond surfaces underwent rigorous structural analysis. Low energy electron diffraction (LEED) revealed that clean (111) diamond surfaces exhibit 1X1 patterns under vacuum. Annealing the sample above 1000 C causes reconstruction to a 2X2/2X1 indistinguishable pattern, rather than spontaneous graphite formation[13].

Studies involving photon stimulated ion desorption (PSID) and vibrational low energy electron loss spectroscopy (EELS) brought to light the surface effects of hydrogen. An unreconstructed (111) 1X1 diamond surface is hydrogen terminated, whereas the reconstructed surface is virtually hydrogen free. Reconstruction occurs at

the threshold temperature for hydrogen desorption, suggesting that hydrogen inhibits surface relaxation. Furthermore, treating the reconstructed (111) diamond surface with atomic hydrogen, instead of molecular hydrogen, below the 1000 C transition temperature, restored the surface to its original unreconstructed state. Hence, atomic hydrogen adsorption/ desorption coupled directly with the unreconstructed/ reconstructed diamond surface states[13].

Not contented yet, Pate explored the chemical nature of reconstruction via surface-vibrational EELS. When hydrogen bonded to the diamond surface, carbon hybridized in an  $sp^3$  configuration. After reconstruction, the hydrogen deficient surface relaxed toward  $sp^2$  hybridization[13].

Reflecting back to the Russian work, Pate applied his fundamental surface information to chemical vapor deposition. For diamond substrates, the Russians obtained polycrystalline films below 750 C, epitaxial films with increasing growthrate as the substrate temperature ranged between 750 and 1000 C, and level growthrate with enhanced graphitic inclusions as films exceeded the 1000 C temperature barrier. The rationale behind this data could be explained in the following way: Below 750 C, the diamond substrate is saturated with hydrogen, so crystallites grow disoriented relative to the substrate and eventually terminate themselves due to the excess atomic hydrogen present in the growth environment. Between 750 and 1000 C, the hydrogen evolves from the surface making an increasing number of epitaxial sites available as the temperature rises; however, the residual atomic hydrogen stabilizes the growth surface to  $sp^3$  hybridization. Beyond 1000 C, the residence time of the atomic hydrogen on the growth plane is too short to maintain the  $sp^3$  hybridization, so surface relaxation leads to graphitic inclusions[13].

Pennsylvania State researchers performed intense transmission electron microscopy (TEM) and Raman spectroscopy on microwave plasma CVD films to determine the origin of graphite formation. Although no definitive answers came out of the study, they recognized some interesting trends pertaining to heteroepitaxy:

(i) Below .5 mol % methane concentration, no graphite or other nondiamond features appeared in the films grown near 1000 C. However, planar defects such as stacking faults and twinning were visible on the {111} planes. For a 2 mol % methane dilution, graphite preferentially grew on or close to the {111} planes of diamond in a highly ordered fashion. Above 5 mol % methane, graphite crystallites took on a random distribution relative to the {111} diamond planes.

(ii) Optimum growth temperatures centered around 1000 C. Lower temperatures favored amorphous carbon, whereas higher temperatures enhanced graphite inclusions. Grain boundaries provided attractive sites for graphite nucleation and further growth up to a few hundred angstroms in diameter.

(iii) Diamond near a foreign substrate interface possessed more graphite and nondiamond components than its growth side. Later evidence revealed a homogeneous diamond profile if the foreign surface contained diamond seed crystals. Although it stands to reason that diamond nucleates and grows on itself easier than foreign substrates, it's unclear why other forms of carbon initially grow on unseeded substrates, but eventually give way to diamond deposition.

(iv) Whether the foreign substrate was silicon, silica, or tungsten carbide, the graphite profiles had similar behavior as far as TEM could discern[14].

Scientists at the Physical Chemistry Department of General Motors were so intrigued by the surface phenomenon associated with diamond heteroepitaxy, that they coupled a hot filament CVD system to a characterization chamber. Although no real time measurements could be made, they had the capability to transfer their sample back and forth between the growth chamber and the surface analysis system entirely under vacuum. Surface characterization included: x-ray photoelectron spectroscopy (XPS), electron energy loss spectroscopy (EELS), x-ray excited Auger electron spectroscopy (XAES), and low energy electron diffraction (LEED) [15,16].

A detailed surface analysis was carried out on the substrates prior to growth to

assure cleanliness and serve as a baseline. Thereafter, the same characterizations were performed at routine growth stages throughout the run. The two substrates they chose to examine were Si(100) and Ni(100) [15,16].

For the silicon sample, XPS identified an  $\text{SiO}_2$  overlayer and carbon residue before growth. Fifteen minutes into the run, both contaminants are removed and replaced by a distinct SiC layer. After 4.5 hours, diamond nucleation takes place as the SiC layer approaches 90 angstroms. From then on, diamond grows through the completion of the run at 17 hours[15,16].

In the case of nickel, four distinct growth phases appear. Initially, carbon coats the substrate in an ordered c(2X2) array covering only half the hollow sites. Then, graphite deposits in a disorderly fashion as islands on top of the c(2X2) surface. As the graphite disorder enhances, the surface takes on an amorphous/ glassy carbon structure. Finally, diamond nucleation and growth occurs on the amorphous/ glassy carbon surface[15,16].

For the same process conditions, SiC, ordered carbon, graphite, amorphous/ glassy carbon, and diamond can grow depending exclusively on the surface state. Although nickel substrates have lattice constants close to diamond, the diamond never makes contact with the nickel or the ordered c(2X2) surface for hopes of epitaxy[15,16]. Clearly, a complex set of kinetic and/or thermodynamic factors influence the ultimate material growth. Perhaps we should take a look at some proposed diamond growth mechanisms.

### ***Mechanisms***

Despite a few promising leads, no single proposal can fully explain all the observations associated with diamond film growth. Rather than accept one mechanism, some people favor a variety of growth pathways which operate in parallel, depending on gas excitation, pressure, or surface sites available for diamond growth. This section will attempt to review the experimental data and introduce theory which supports these observations; however, any conclusions shall be left to the reader.

Although surface bombardment may serve to stabilize metastable diamond growth, scientists at Case Western Reserve University caution that the threshold displacement energy for diamond is about 75 eV. Ion or neutral collisions exceeding the threshold limit can disrupt carbon atoms on the surface, leading to diamondlike material rather than real diamond. Below the threshold limit, particles hitting the surface could enhance adatom mobility and thereby promote diamond crystallization[3].

Vapor deposited diamond is plagued by defects, most commonly stacking faults and multiple twins. To appreciate why, look at the diamond structures in figures 8 and 9, then compare them to the twinned structures in figure 13. Clearly, a boat type carbon ring coincides with the twin plane. In the structure section, the appearance of boat shaped rings implied eclipsed carbon bonds leading to hexagonal diamond. Since the energy difference between staggered and eclipsed carbon bonds is relatively small on {111}surfaces, twinning readily takes place if hexagonal carbons replace cubic sites. As figure 13b illustrates, two twin planes in parallel essentially create a stacking fault. Multiply twinned crystals appear frequently as decahedrons and icosahedrons, having five and twenty symmetric twin planes[3].

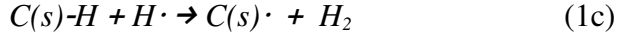
A general mechanism sequence might start off with an endothermic dissociation of molecular hydrogen,



Although this step consumes a substantial amount of energy, excitation sources such as plasmas or hot filaments have ample supply. Once the energy is expended, all subsequent reactions are exothermic. For instance, an atomic hydrogen may choose to fill a vacant surface site,



Energetically, the H-H bond is preferred over any C-H bonds, so quite frequently atomic hydrogen attacks surface sites or gaseous hydrocarbons,



Ultimately, the flux of gaseous free radicals hitting surface free radicals leads to an addition reaction,



Applying steady-state kinetics to the above system of reactions then yields a diamond growthrate proportional to a product between  $H\cdot$  and  $R\text{-H}$  concentrations, which agrees favorably with preliminary rate studies[3].

As simple as this model appears, it reveals the necessity for superequilibrium amounts of atomic hydrogen. In its thermodynamic quest to realize molecular hydrogen, atomic hydrogen: i) attaches to vacant surface sites, preventing reconstruction or graphitization, and ii) plays an active role in creating free radicals on the film surface or in the gas phase, leading to growth. Although  $C_2H_2$  and  $CH_3$  have been suggested as potential growth species,  $R\cdot$ , this subject deserves further attention[3].

### ***Electrochemical benchmarks***

Since diamond films came into existence about 25 years ago, its electronic properties as a polycrystalline structure has taken on a prominent role as an electrode material, despite its shortcomings in attaining semiconductor status, where single crystal morphology is desired. A typical electrochemical cell[17] would look something like figure 14, made of glass, with an o-ring seal at the bottom to interface with the working electrode of interest. Note that this configuration avoids the requirement of making a dipstick from circuit board stock, since the electrical contacts can be kept out of solution. Diamond films for these purposes are grown on highly doped Si wafers to permit sufficient electrical conductivity to the back of the wafer. The back of the Si wafer is scratched and a bead of Ag paste is applied to make contact to a Cu or Al metal plate. The other peripheral components which complement a normal electrochemical cell

include: a port for gas purge, a counterelectrode opening, and reference electrode entry.

In the absence of grain boundaries, dopants, or structural defects, diamond films behave primarily as an insulator, with a band gap on the order of 5.5 eV. Since insulating electrodes show very little electrochemical activity, it is necessary to lace the film with boron on the ppm scale before any practical electron transfer becomes significant. A proposed band diagram for a diamond thin film/ solution interface looks something like figure 15. It is believed that the B atom wavefunctions overlap to the extent that a bands accumulate in the center of the bandgap of diamond, with electron transfer occurring in the closest valence or conductance band, depending on whether a reduction or oxidation takes place in solution[17].

### ***Nanocrystal barrier***

As the last paragraph foretold, grain boundaries and structural defects can create more electron pathways in the middle of diamond's bandgap to enhance the electron transfer capabilities to the redox couple[17]. Consequently, nanocrystalline diamond films could replace microcrystalline morphology, once the growth conditions to influence grain size became known[18]. A 1 mol % CH<sub>4</sub>/ 99 mol % H<sub>2</sub> fairly consistently produced a diamond grain size up to 100 micrometers; whereas, the nominal grain size could be scaled down to about 20 nanometers by changing the gas mixture to 1 mol % CH<sub>4</sub>/ 5 mol % H<sub>2</sub>/ 94 mol % Ar. Again, it should be reinforced that keeping the carbon to hydrogen flow ratio as low as possible insures that sp<sup>2</sup> graphitic inclusions be kept to a bare minimum through a 10:1 selective etch rate of graphite over diamond.

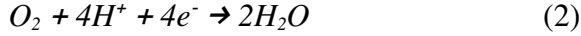
However, the dangling bonds on the grain boundaries create a pi network of sp<sup>2</sup> coordinated carbons, which enhance the electron transfer along the periphery of the crystallites. Hence, by scaling down the grain size, you increase the magnitude of grain boundary conduction pathways. If you then dope the evolving crystals with boron during film growth, the electrons have a conduction channel through the grain, in addition to the boundary layer path[18].

So, why would one want to use polycrystalline diamond electrodes in the first place? Relative to glassy carbon, the standard for passive catalytic activity, diamond thin films have a larger window of potential range, as figure 16 demonstrates, with a rather featureless cyclic voltammogram in 1 M KCl background electrolyte, which is stable over multiple cycles. This property alone accounts for a superior signal to background ratio (sbr) in electroanalytical measurements, in comparison with glassy carbon. In addition: (i) light transparency can be useful for optical electrodes, (ii) hardness characteristics preclude electrode pretreatment like polishing, and (iii) inertness allows exposure to the harshest electrochemical environments without deterioration in battery/fuel cell applications[18].

### *Platinum/ diamond composite*

In the same vein that precious metals coat the surface of a support material to minimize cost and maximize surface area in a catalytic process, diamond thin films can be impregnated with Pt, in accordance with a procedure like figure 17. A polycrystalline boron doped diamond thin film is grown over a bare silicon wafer. Then using a electrodeposition technique, the Pt is distributed as diffusely as possible to optimize contact area. Because the Pt adherence to diamond is weak, a subsequent diamond overlayer secures the Pt in place, with diamond growth preferential to the surrounding diamond matrix[19].

Since the secondary diamond thin film buries some of the smaller Pt particles, and surrounds the sides of the larger Pt islands, there is a commensurate loss in overall Pt surface area, as evidenced by figure 18, a cyclic voltammogram before and after the diamond overlayer. In a 0.1 M HClO<sub>4</sub> solution, the dashed line, traced by an electrode with a diamond overlayer, has smaller oxidation/ reduction peak intensity, and a slightly narrower voltage window, relative to the electrode without a diamond overlayer. In figure 19, when a Pt/ diamond composite electrode, curve A, is compared to a pure Pt foil, curve B, the performance is almost identical for the oxygen reduction reaction:



Curve C represents the response of a boron doped diamond film, under similar oxygen saturated conditions, in a 0.1 M perchloric acid solution[19].

### *sp<sup>2</sup> impurity level*

Figure 20 illustrates how the topography of a boron doped diamond thin film is influenced by changing the C/H ratio, shorthand for methane to hydrogen gas flow ratio, in the range of 0.3 to 5 vol %. Such a proposal would ultimately change the level of sp<sup>2</sup> graphitic inclusions in the film, to see how that might effect electrode characteristics. As the atomic force microscope landscape reveals, increasing the C/H ratio causes proportionately larger secondary nucleation, driving down the grain size, while enhancing film uniformity[20].

The extent of sp<sup>2</sup> carbon incorporation can be calibrated with a Raman spectra, as in figure 21. A first order phonon mode occurs for: Si at 514 cm<sup>-1</sup>, diamond at 1332 cm<sup>-1</sup>, and sp<sup>2</sup> carbon in the range of 1500 to 1590 cm<sup>-1</sup>. As the C/H ratio increases, the Si and diamond peaks diminish, and give rise to sp<sup>2</sup> carbon, until it reaches 5 vol %, where a mixture of sp<sup>2</sup> and sp<sup>3</sup> carbon prevails, characteristic of glassy carbon. Further confirmation of the carbon phase becomes evident within the context of figure 22, using cyclic voltammetry, in 0.1 M perchloric acid, as a background electrolyte. In accordance with higher C/H ratios, the potential window diminishes and the background current increases, until the CV matches glassy carbon[20].

Within the framework of redox couples, two major reaction types transpire. Namely, *outer sphere* interactions refer to reactions that only depend on the diffusion of the redox species to and from the electrode, independent of surface morphology, where the electrode acts solely as a source or sink for electrons. Therefore, only the density of states at the formal potential comes into play for such an interaction. Alternatively, *inner sphere* phenomenon relies dramatically on surface topography, influencing surface kinetics near the interface, for such processes like adsorption. In this scenario, diffusion

of redox species, surface conditions, and density of states all contribute to the effect[20].

Now that we've established some guidelines, let's consider some traditional oxidation/ reduction species, for progressive levels of  $sp^2$  carbon, in the diamond electrode. Among the redox systems tested, only  $\text{Ru}(\text{NH}_3)_6^{3+/2+}$  behaves in an outer sphere manner, as figure 23 attests. In contrast, it would be tempting to conclude figure 24 depicts outer sphere characteristics; however, seasoned electrochemists should recognize that  $\text{Fe}(\text{CN})_6^{3-/4-}$  possesses inner sphere qualities, dependent on whether diamond is hydrogen or oxygen terminated, or the amorphous carbon film contains exposed clean edge planes. Hence, the consistent kinetic behavior testifies to the relatively pristine and inert surface structure, measured by  $\Delta E_p$ , within the range of 60 to 90 mV, among all the carbon films. For a completely reversible reaction, the change in the peak current potentials should scale with  $59/n$  mV [20].

On the other hand, figures 25 and 26, representative of  $\text{Fe}^{3+/2+}$  and 4-*tert*-butylcatechol, respectively, exhibit sluggish surface kinetics, except for the glassy carbon phase. In the case of  $\text{Fe}^{3+/2+}$ , carbonyls form on the surface of glassy carbon from water or air, accelerating the Fe absorption mechanism. Pi-pi interactions between glassy carbon and 4-*tert*-butylcatechol appears to favor surface interactions, relative to diamond. Thus, a battery of inner sphere redox couples can probe for surface states, contaminants, and morphology based on known reaction mechanisms[20].

### **Boron dopant role**

Finally, I would like to draw the reader's attention to a paper by Holt[21], who tackles the controversial issue surrounding the charge transfer mechanism on boron doped diamond films. In it, she presents the two proposed charge transfer mechanisms, one in which electrons diffuse to the surface from defect centers, where one would expect a relatively homogeneous electrochemical activity. The alternative states that localized inhomogeneities from defects results in stratification of electrochemical activity, perhaps reflecting the film morphology and dopant distribution. In this proposal, one could

envision a random array of microelectrodes, when the diffusion length is short, ranging to a uniform electrode, if the diffusion length is long. Using a number of surface topology electrochemical measurements, in combination with computer simulations, Holt attempts to elucidate the true nature of charge transfer. For the boron doping concentrations considered, up to 10 ppm, she concludes that the inhomogeneous mechanism prevails, but she does not rule out the homogeneous mechanism at higher doping levels.

### ***Conclusion***

Metastable diamond films became possible through atomic hydrogen, energized in plasmas or hot filaments, which selectively etches  $sp^2$  carbon 10 times more effectively than  $sp^3$  carbon. Although semiconductor diamonds have yet to find realization in single crystalline form, polycrystalline diamond films provide the necessary framework for suitable electrodes, possessing optical transparency, hardness, and chemical inertness. A number of electrochemical tests can determine surface states, contamination levels, and structural information.

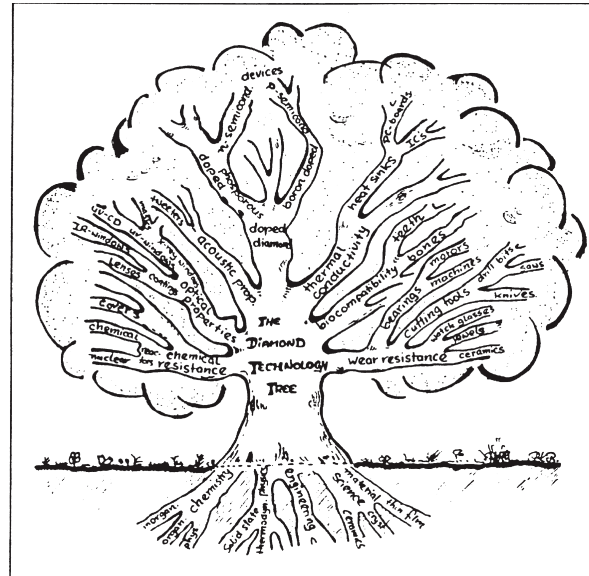


**Figure 1:** Scientific roots and application branches in the "diamond technology tree."

| Properties                                      | Diamond | Si    | $\beta$ -SiC |
|---|---------|-------|--------------|
| Band gap (eV)                                   | 5.5     | 1.1   | 3.0          |
| Carrier mobility ( $\text{cm}^2/\text{V.sec}$ ) |         |       |              |
| Electron  | 1,800   | 1,500 | 400          |
| Hole  | 1,600   | 600   | 50           |
| Dielectric constant                             | 5.5     | 11.8  | 9.7          |
| Thermal conductivity ( $\text{W/cm K}$ )        | 20      | 1.5   | 5            |
| Absorption edge ( $\mu\text{m}$ )               | 0.2     | 1.4   | 0.4          |
| Hardness ( $\text{kgm/mm}^2$ )                  | 10,000  | 1,000 | 3,500        |
| Lattice Constant ( $\text{\AA}$ )               | 3.567   | 5.430 | 4.358        |
| Density ( $\text{gm/cm}^3$ )                    | 3.515   | 2.328 | 3.216        |
| Refractive Index                                | 2.42    | 3.5   | 2.65         |

**Figure 2:** Diamond properties compared to silicon and beta-silicon carbide.

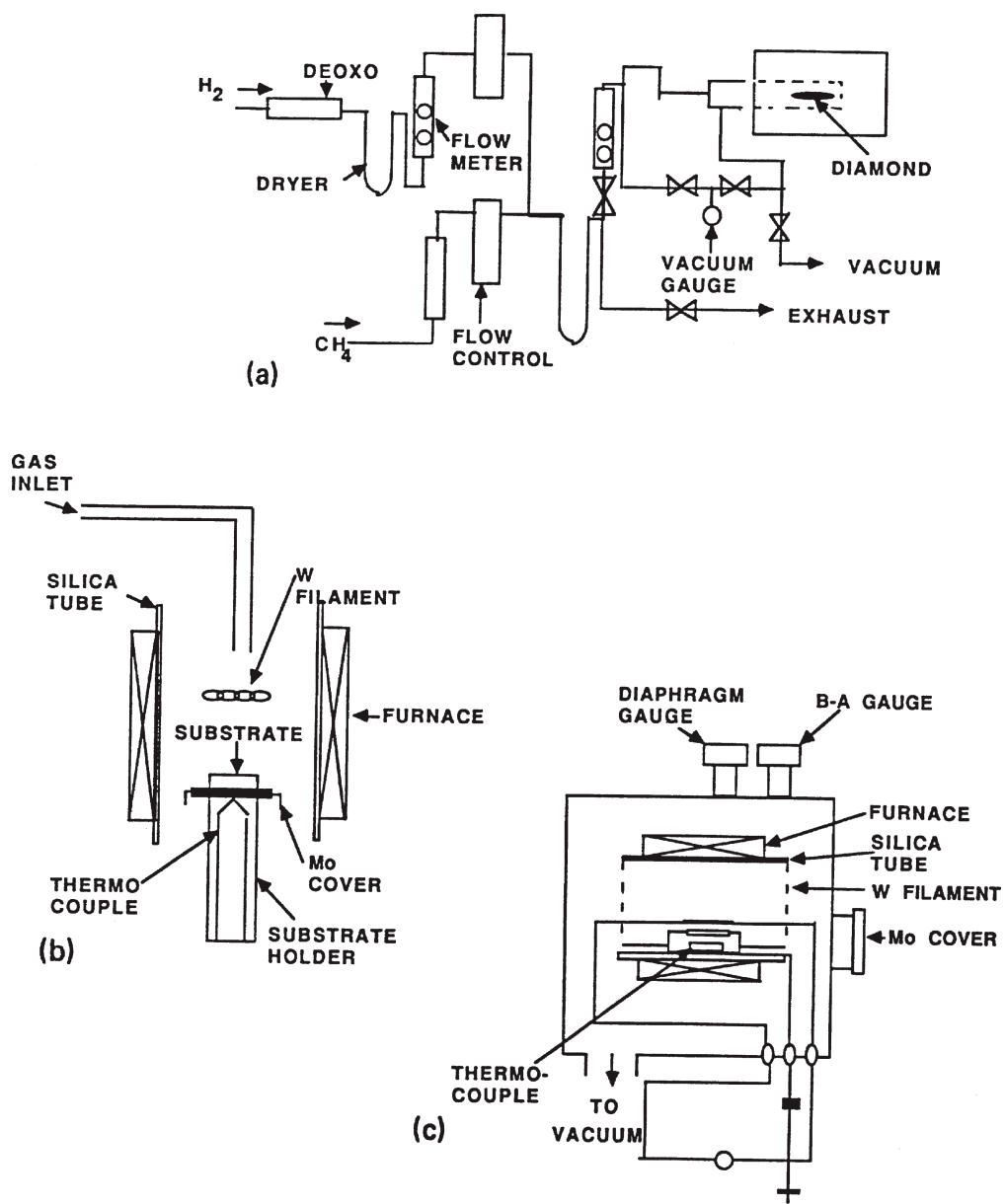


**Figure 3:** Thermal CVD apparatus; (a) chemical vapor transport, (b) hot filament CVD, and (c) electron assisted CVD.

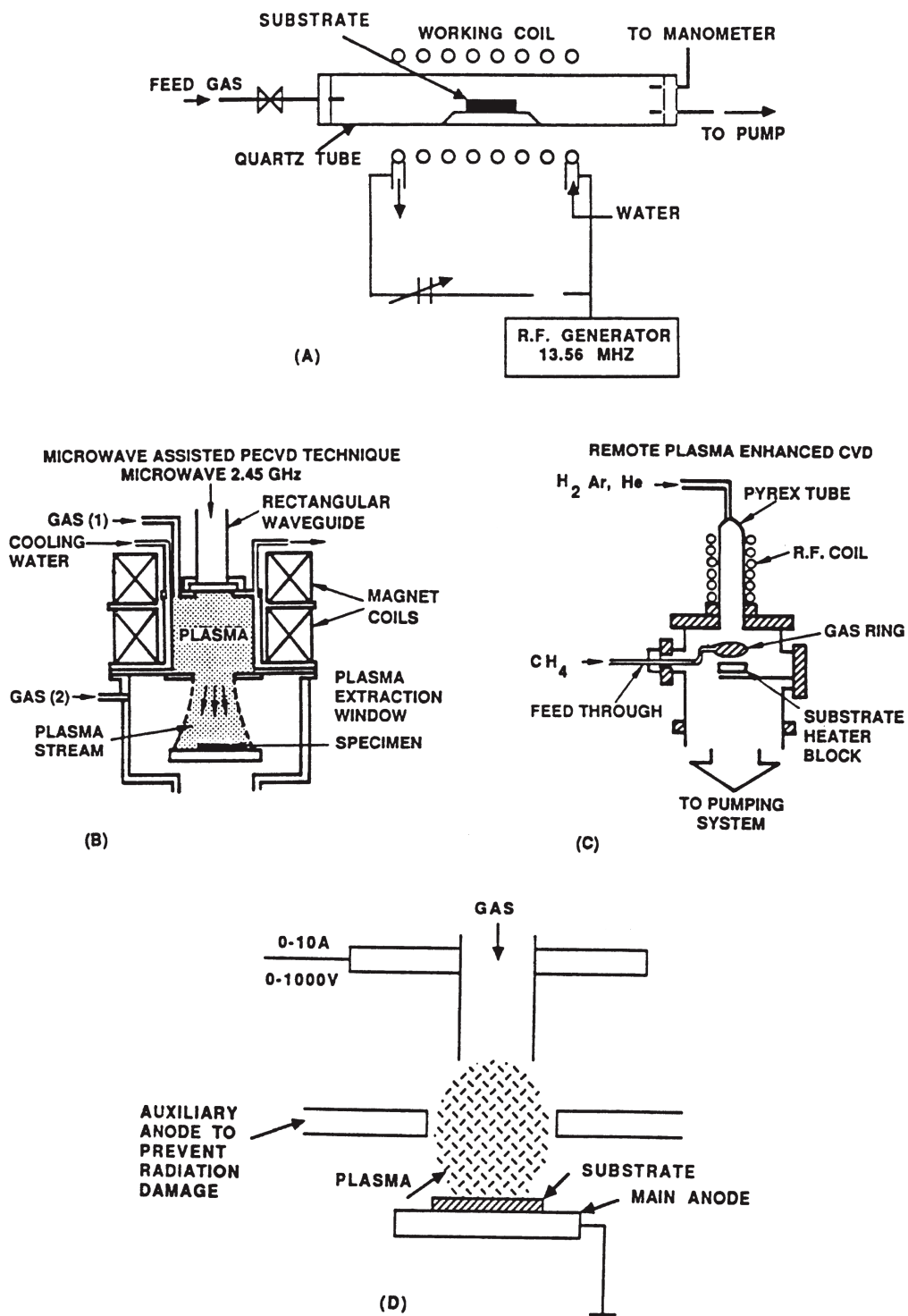


**Figure 4:** Plasma CVD systems; (a) RF excitation, (b) magneto assisted microwave, (c) remote RF, and (d) hollow cathode.

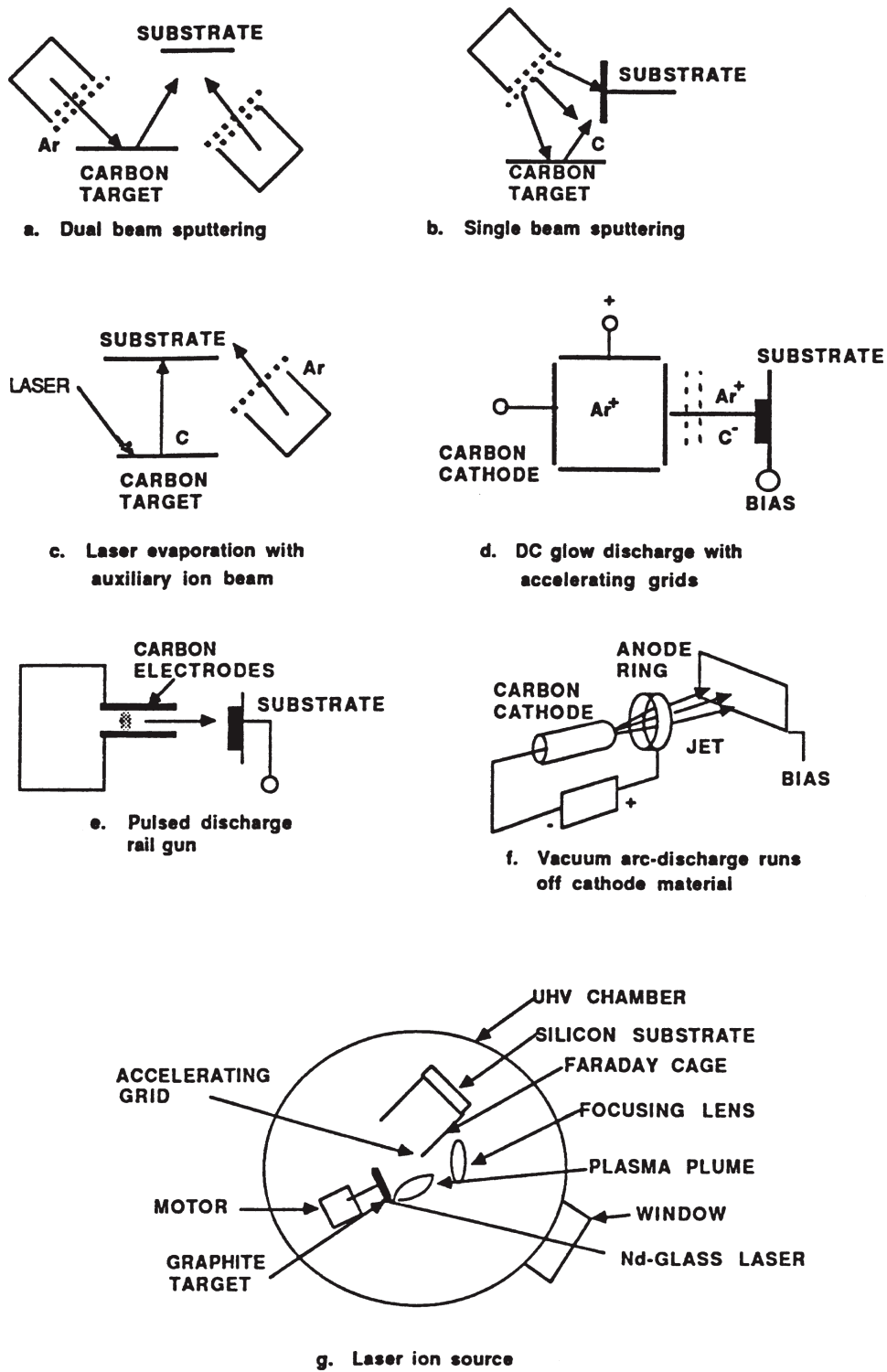


**Figure 5:** Ion beam deposition methods.

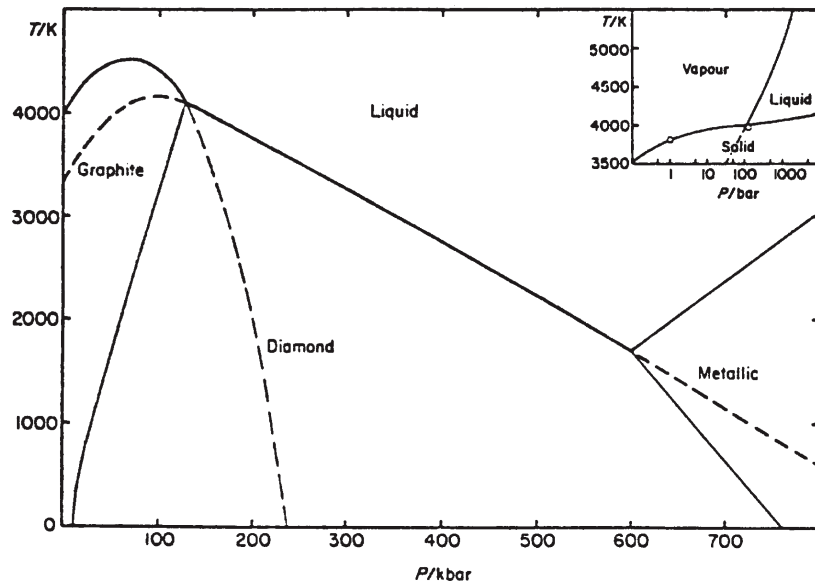


**Figure 6:** Most probable carbon phase diagram.

| Material | Stable phase | Metastable phase | Substrate | Reference |
|----------|--------------|------------------|-----------|-----------|
| Nb,Nb    | $A\ 2$ (bcc) | $A\ 15$          | Nb,Ge     | a         |
| Co       | $A\ 3$ (hcp) | $A\ 2$ (bcc)     | GaAs      | b         |
| Fe       | $A\ 2$ (bcc) | $A\ 1$ (fcc)     | Cu        | c         |
| Sn       | $A\ 5$ (tet) | $A\ 4$ (dc)      | CdTe      | d         |
| Nb       | $A\ 2$ (bcc) | $A\ 1$ (fcc)     | MgO       | e         |
| Ti       | $A\ 3$ (hcp) | $A\ 2$ (bcc)     | NaCl      | f         |

<sup>a</sup>G. R. Stewart, L. R. Newkirk, and F. A. Valencia, Phys. Rev. B **21**, 5055 (1980).

<sup>b</sup>G. A. Prinz, Phys. Rev. Lett. **54**, 1051 (1985).

<sup>c</sup>W. A. Jesser and J. A. Matthews, Philos. Mag. **15**, 1097 (1967).

<sup>d</sup>R. F. C. Farrow, D. S. Robertson, G. M. Williams, A. G. Cullis, G. R. Jones, I. M. Young, and P. N. J. Dennis, J. Cryst. Growth **54**, 507 (1981).

<sup>e</sup>T. E. Hutchinson and K. H. Olsen, J. Appl. Phys. **38**, 4933 (1967).

<sup>f</sup>F. E. Wawner and K. R. Lawless, J. Vac. Sci. Technol. **6**, 588 (1969).

**Figure 7:** Successful examples of metastable film crystallization.

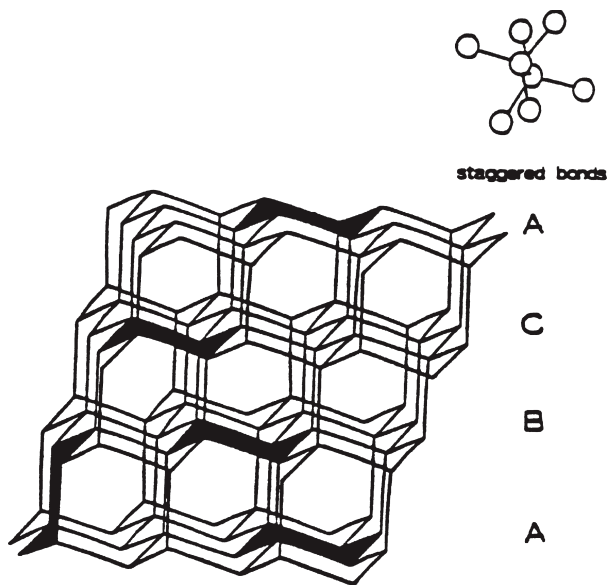


**Figure 8:** Diamond cubic lattice.

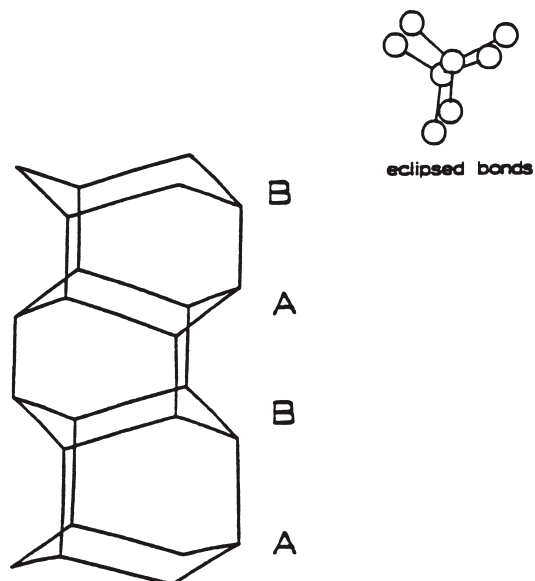


**Figure 9:** Lonsdaleite (or hexagonal diamond) lattice.

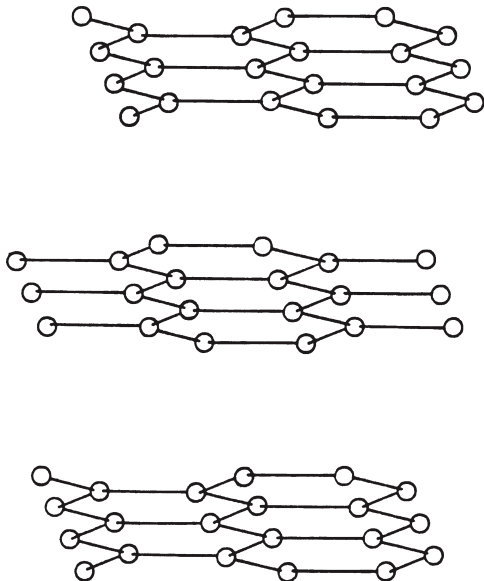


**Figure 10:** Graphite structure.

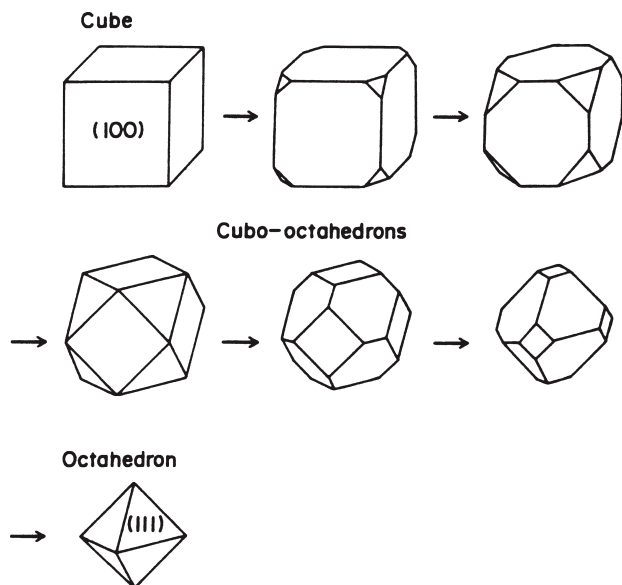


**Figure 11:** Polyhedral diamond morphology; usually only upper half of each representation appears on the substrate due to surface wetting.

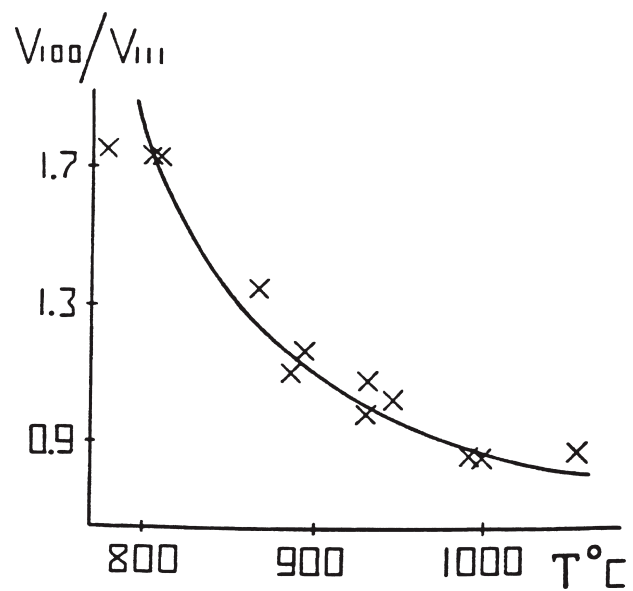


**Figure 12:** Crystal habit versus substrate temperature.

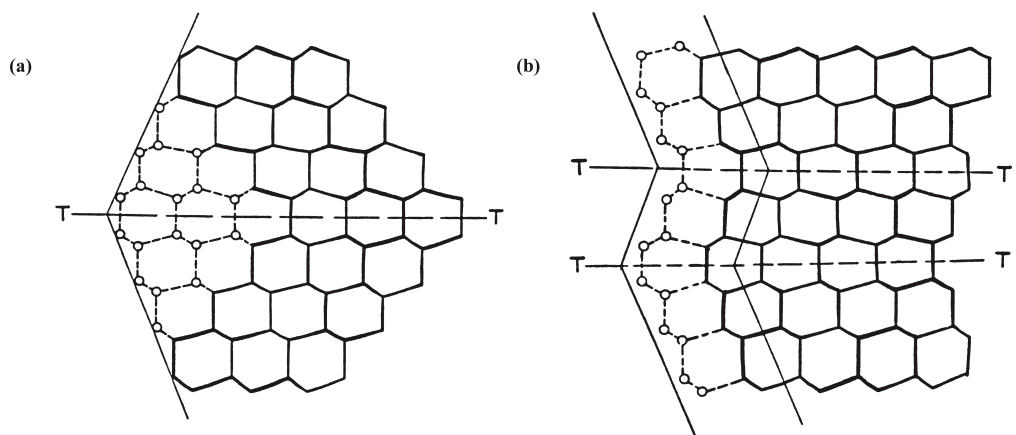


**Figure 13:** Growth defects; (a) single twin plane (T-T) changes stacking sequence and (b) two sequence errors form a stacking fault.

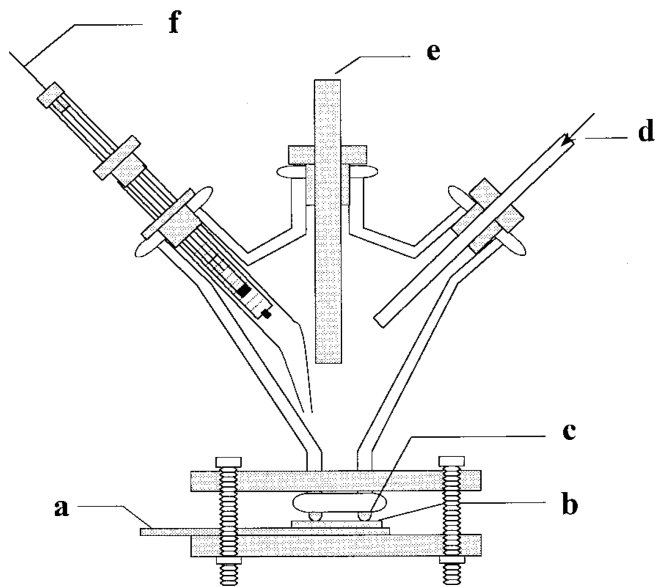


**Figure 14:** Electrochemical cell; (a) collector plate, (b) working electrode, (c) o-ring seal, (d) purge gas, (e) counter electrode, and (f) reference electrode.

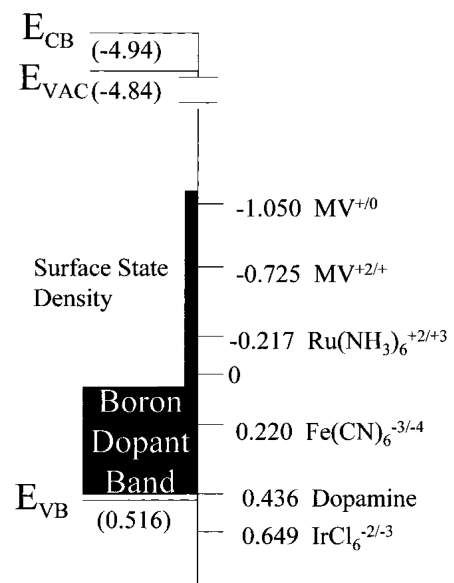


**Figure 15:** Proposed band diagram for interface between diamond and electrolyte.

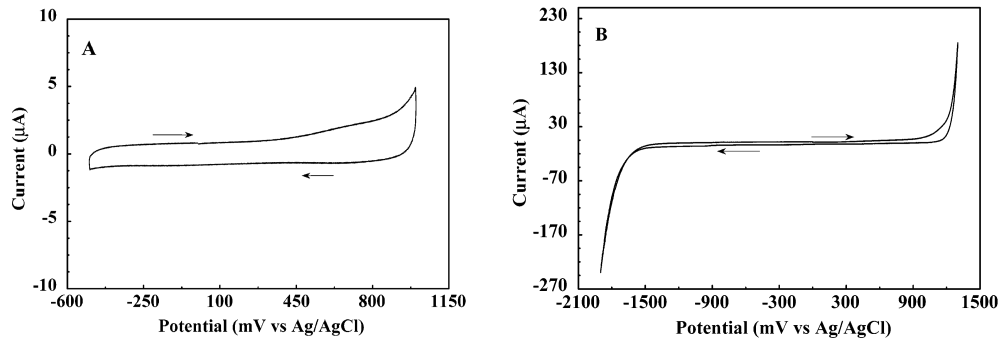


**Figure 16:** Cyclic Voltammogram of nanocrystalline diamond electrode in 1 M KCl over (a) narrow range and (b) working potential window.

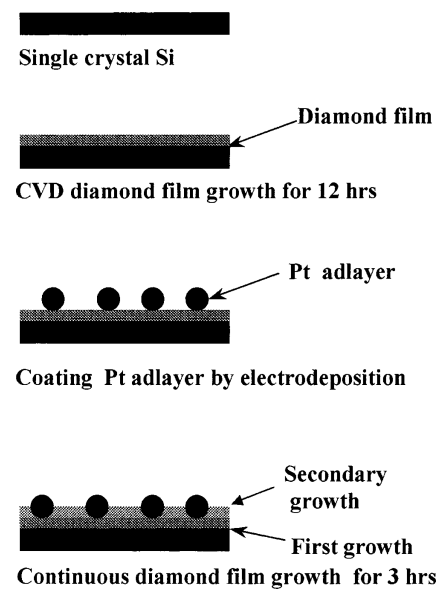


**Figure 17:** Process sequence for Pt/ diamond composite electrode.

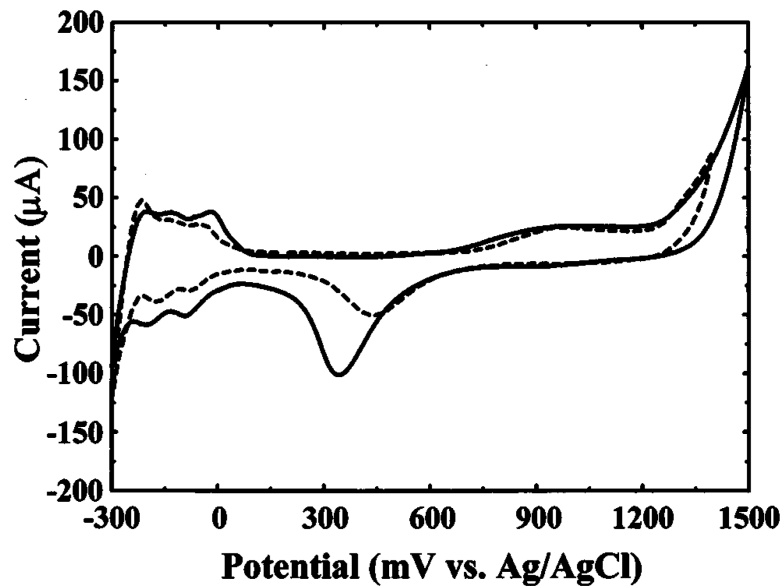


**Figure 18:** Cyclic voltammogram of Pt/ diamond composite electrode in 0.1 M  $\text{HClO}_4$  before (solid) and after (dash) diamond overgrowth layer.

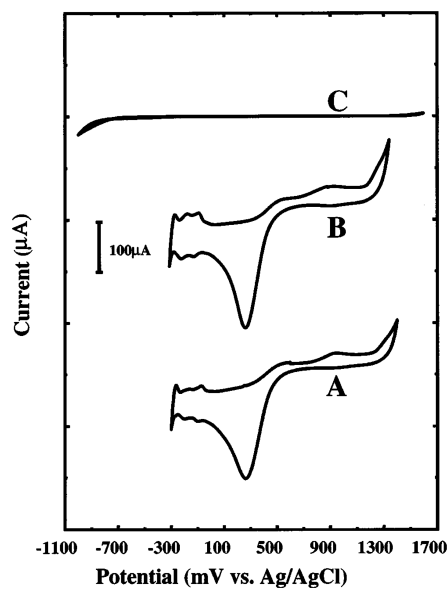


**Figure 19:** Cyclic voltammogram comparison between; (a) Pt/ diamond composite electrode, (b) Pt foil, and (c) bare diamond electrode.

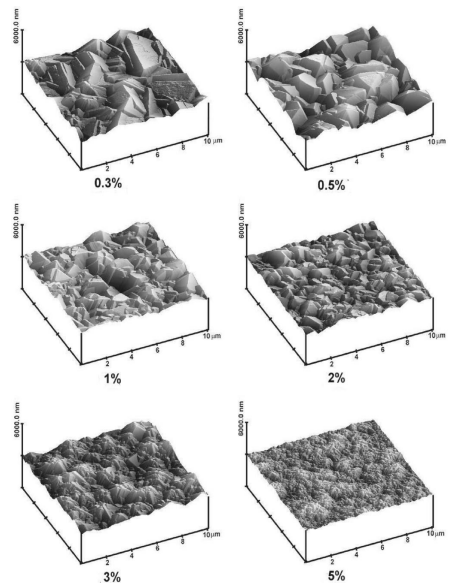


**Figure 20:** Atomic force micrographs for varying C/H flow ratios.

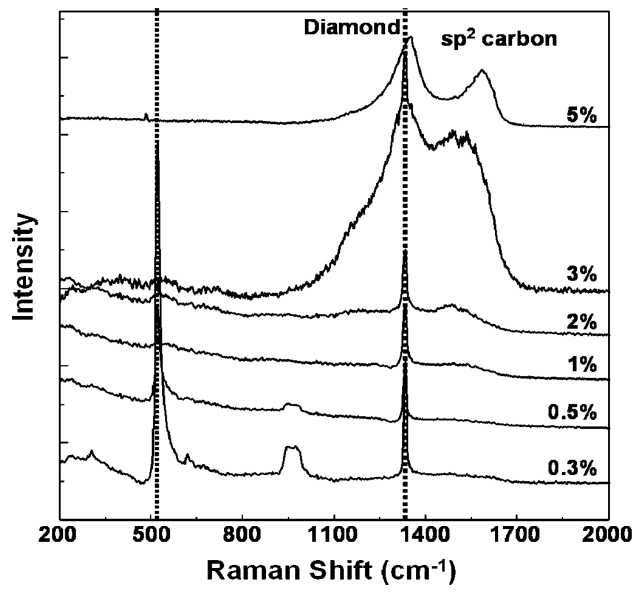


**Figure 21:** Raman spectra as a function of C/H flow ratios.

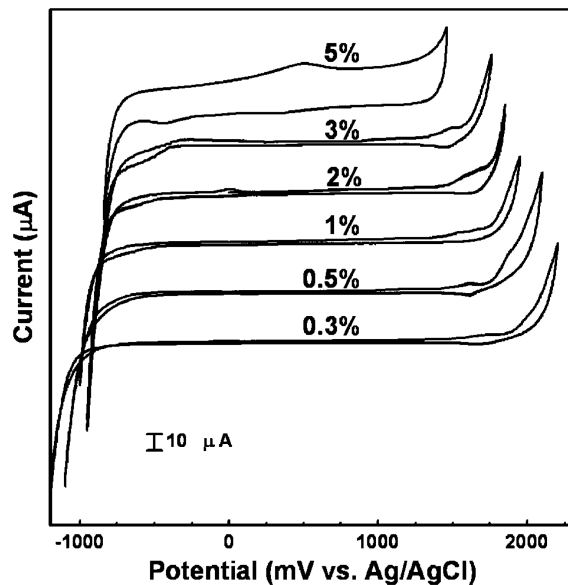


**Figure 22:** Background cyclic voltammograms for the assortment of C/H flow ratios in 0.1 M  $\text{HClO}_4$ .

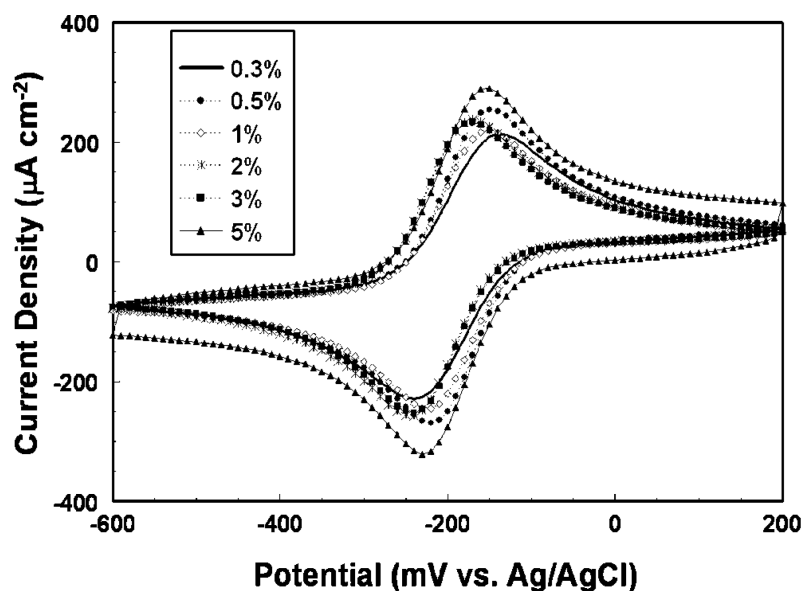


**Figure 23:** Cyclic voltammogram C/H series for 1 mM  $\text{Ru}(\text{NH}_3)_6^{3+/2+}$  in 1 M KCl.

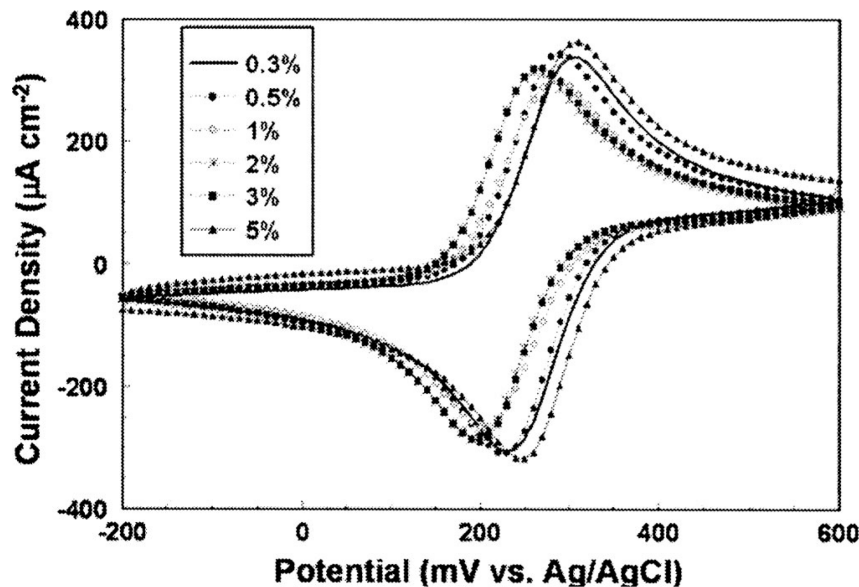


**Figure 24:** Cyclic voltammogram C/H series for 1 mM  $\text{Fe}(\text{CN})_6^{3-/4-}$  in 1 M KCl.

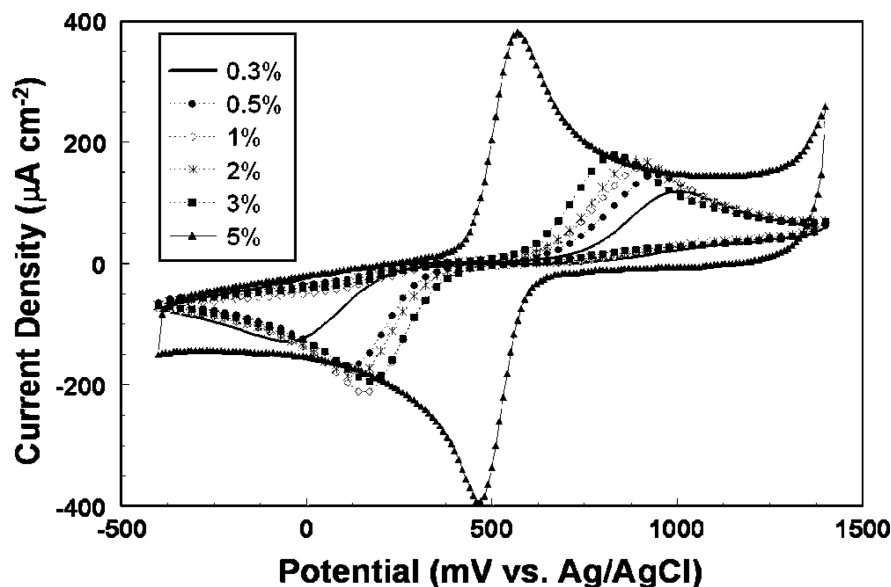


**Figure 25:** Cyclic voltammogram C/H series for 1 mM  $\text{Fe}^{3+/2+}$  in 0.1 M  $\text{HClO}_4$ .

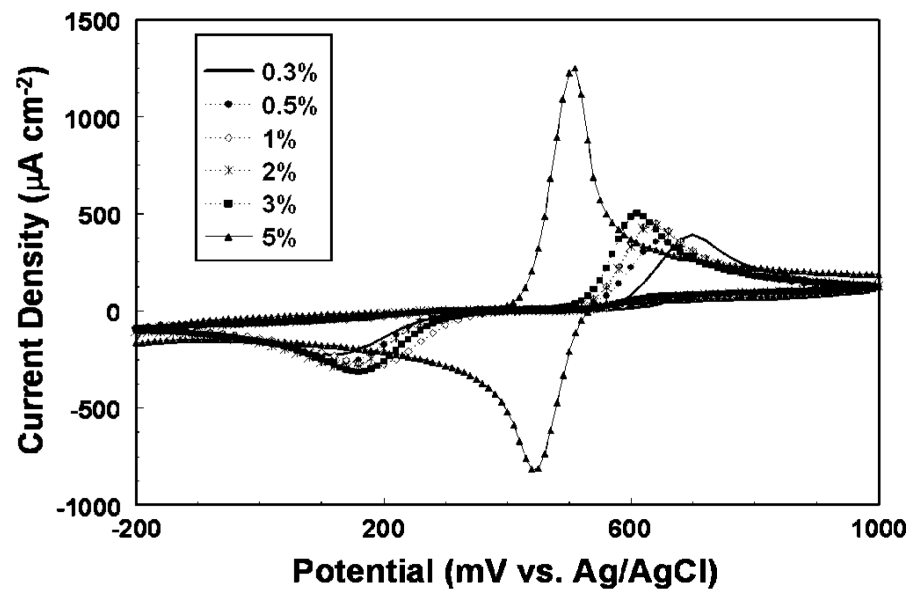


**Figure 26:** Cyclic voltammogram C/H series for 1 mM 4-*tert*-butylcatechol in 0.1 M  $\text{HClO}_4$ .

### References

- [1] C. V. Deshpandey and R. F. Bunshah, *Journal of Vacuum Science and Technology*, **A7**, 2294 (1989).
- [2] R. Messier, et al., *Journal of Metals*, **39**, 8 (1987).
- [3] J. C. Angus, et al., *MRS Bulletin*, **XIV**, 38 (1989).
- [4] E. S. Machlin, *Journal of Materials Research*, **3**, 958 (1988).
- [5] A. P. Malshe, et al., *Journal of Materials Research*, **4**, 1238, (1989).
- [6] A. R. Badzian, et al., *E-MRS Meeting*, **XV**, 63 (1987).
- [7] N. Setaka, *Journal of Materials Research*, **4**, 664 (1989).
- [8] K. Suzuki, et al., *Applied Physics Letters*, **50**, 728 (1987).
- [9] K. Katsuki, et al., *Applied Physics Letters*, **49**, 634 (1986).
- [10] H. Kawarada, K. S. Mar, and A. Hiraki, *Japanese Journal of Applied Physics*, **26**, L1032 (1987).
- [11] S. Matsumoto, M. Hino, and T. Kobayashi, *Applied Physics Letters*, **51**, 737 (1987).
- [12] B. V. Spitsyn, L. L. Bouilov, and B. V. Derjaguin, *Journal of Crystal Growth*, **52**, 219 (1981).
- [13] B. B. Pate, *Surface Science*, **165**, 83 (1986).
- [14] W. Zhu, et al., *Journal of Vacuum Science and Technology*, **A7**, 2315 (1989).
- [15] D. N. Belton, et al., *Applied Physics Letters*, **54**, 416 (1989).
- [16] D. N. Belton and S. J. Schmieg, *Journal of Applied Physics*, **66**, 4223 (1989).
- [17] M. C. Granger, et al., *Analytical Chemistry*, **72**, 3793 (2000).
- [18] Y. Show, et al., *Chemistry of Materials*, **15**, 879 (2003).
- [19] J. Wang and G. M. Swain, *Journal of the Electrochemical Society*, **150**, E24 (2003).
- [20] J. A. Bennett, *Journal of the Electrochemical Society*, **151**, E306 (2004).
- [21] K. B. Holt, *Journal of Physical Chemistry B*, **108**, 15117 (2004).